Journal of
Composites Science

MDPI

Article

Competitive Adsorption of Aqueous Cd(II) and Pb(II) Solutions onto Silicas Synthesized with Saponin as Template Agent

Claudia-Maria Simonescu [1], Florina Dumitru [1,*], Bianca Zărnescu [1], Daniela Cristina Culiţă [2], Anca Răzvan [1], Ovidiu Oprea [1,3,4,5], Roxana Truşcă [3] and Eugeniu Vasile [1]

[1] Faculty of Chemical Engineering and Biotechnologies, National University of Science and Technology Politehnica Bucharest, 1-7 Polizu St., 011061 Bucharest, Romania; claudia.simonescu@upb.ro (C.-M.S.); zarnescubianca@yahoo.com (B.Z.); anca.razvan@upb.ro (A.R.); ovidiu.oprea@upb.ro (O.O.); eugeniuvasile@yahoo.com (E.V.)
[2] Ilie Murgulescu Institute of Physical Chemistry, Romanian Academy, 202 Splaiul Independentei, 060021 Bucharest, Romania; danaculita@yahoo.co.uk
[3] National Center for Micro and Nanomaterials, National University of Science and Technology Politehnica Bucharest, Splaiul Independentei 313, 060042 Bucharest, Romania; truscaroxana@yahoo.com
[4] National Research Center for Food Safety, National University of Science and Technology Politehnica Bucharest, Splaiul Independentei 313, 060042 Bucharest, Romania
[5] Academy of Romanian Scientists, Ilfov Street 3, 050044 Bucharest, Romania
* Correspondence: florina.dumitru@upb.ro

Abstract: The aim of the research was to prepare silica adsorbents using an environmentally friendly pathway, a template synthesis with saponin biosurfactant as a structure-directing agent. The adsorbents prepared in this way exhibit improved adsorption properties while maintaining environmental innocuousness. For the preparation of porous silica, the biosurfactant template sol–gel method was used with tetraethoxysilane as a silica precursor. The silica adsorbents were analyzed by FTIR spectroscopy, nitrogen adsorption–desorption and SEM/EDX microscopy, TEM/HRTEM microscopy, and thermogravimetric analyses. Batch tests were carried out to remediate Pb(II)/Cd(II) ions in single/binary aqueous solutions, and the effect of the surfactant on the adsorption properties was assessed. The optimal adsorption parameters (pH, contact time, initial concentration of metal ions) have been determined. The adsorption was fitted using Langmuir and Freundlich adsorption isotherms and kinetic models. Mathematical modeling of the retention process of Pb(II) and Cd(II) ions from binary solutions indicated a competitive effect of each of the two adsorbed metal ions. The experimental results demonstrated that saponin has the effect of modifying the silica structure through the formation of pores, which are involved in the retention of metal ions from aqueous solutions and wastewater.

Keywords: biosurfactant; biosorbent; porous silica; saponin; template synthesis; Pb(II)/Cd(II) ions

Citation: Simonescu, C.-M.; Dumitru, F.; Zărnescu, B.; Culiţă, D.C.; Răzvan, A.; Oprea, O.; Truşcă, R.; Vasile, E. Competitive Adsorption of Aqueous Cd(II) and Pb(II) Solutions onto Silicas Synthesized with Saponin as Template Agent. *J. Compos. Sci.* **2024**, *8*, 227. https://doi.org/10.3390/jcs8060227

Academic Editor: Prashanth Konda Gokuldoss

Received: 1 May 2024
Revised: 7 June 2024
Accepted: 11 June 2024
Published: 16 June 2024

1. Introduction

Pb(II) and Cd(II) ions are priority pollutants according to environmental regulations [1]. As reported by the World Health Organization (WHO), inorganic compounds of lead and cadmium are included in group 2A (by the International Agency for Research on Cancer, https://monographs.iarc.who.int/agents-classified-by-the-iarc/, accessed on 26 April 2024) and are described as "probably carcinogenic" to humans with a maximum permissible concentration of 10 µg/L and 3 µg/L in drinking water [2–4].

Different physicochemical methods for the remediation of wastewater and aqueous solutions containing these metal ions have been developed and applied to reduce their significant negative effects on the environment and human health. The most representative methods are ion exchange, precipitation/coagulation, reverse osmosis, membrane filtration, and electrochemical methods [5]. These traditional methods are burdened by

high implementation costs and disadvantages, such as the generation of large amounts of toxic sludge, use of various chemical substances as raw materials, purification efficiency that does not reach maximum values, high energy consumption, and the production of secondary pollution, that limit their widespread use [5].

Adsorption, with its advantages of low maintenance and reduced handling costs, reusability of the adsorbent materials, high efficiency and selectivity, great diversity of materials that can be used as adsorbents etc., could represent an alternative technology for the removal of heavy metal ions from wastewater. Numerous studies have been carried out on the remediation of Pb(II) and Cd(II) ions in industrial effluents and aqueous solutions by adsorption. The following adsorbent materials have been used: activated carbon and its derivatives [6], clays [7], natural and synthetic zeolites [8,9], hydroxyapatite and its composites [10], hydroxides [11], carbon nanotubes [12], simple and small oxides [13,14], silicates and their derivatives [15,16], magnetic nanoparticles [17–19], lignin and its derivatives [20], chitosan-based materials [21], geopolymers [22], metal-organic compounds [23], food waste [24], agricultural waste [25], industrial waste [26]. Among these, porous materials are considered alternative adsorbents with improved adsorption performance compared to activated carbon and other conventional adsorbent materials. Mesoporous silica with an ordered structure presents a high specific surface area and good physicochemical stability, which allows it to participate in functionalization processes with various functional groups, leading to adsorbents with selectivity and high adsorption capacity. The surface structure of porous and mesoporous silica represents an advantage over other adsorbent materials. It ensures the structural orientation of the host molecules (metal ions) in the pores, which determines the increase in selectivity and adsorption capacity [27]. The synthesis of materials based on porous and mesoporous silica can be carried out by co-condensation, sol–gel methods, wet impregnation, direct incorporation, and alternative methods [28]. The template synthesis method is a relatively simple and easy method that controls the structure, morphology, and pore size through the template material [29]. Surfactants, polymers, and biopolymers are used as template agents [29].

Silica mesoporous compounds are considered intriguing materials for a diversity of applications such as catalysis, biomedicine, drug delivery, and the removal of pollutants [30]. These applications are based on their unique properties, including large surface area, high values of pore volume, non-toxic character, tunable pore size, and surface properties. However, few articles regarding the ability of mesoporous silica-based materials to remove Pb(II) and Cd(II) from aqueous effluents are offered in the literature [31,32].

Our work is focused on the synthesis of novel silica adsorbents using a renewable, readily available, low cost and environmentally benign biosurfactant saponin as a template agent. Saponins are non-ionic biosurfactants, structurally composed of a lipophilic soluble aglycon (steroidal or triterpenoid) and hydrophilic sugar parts that form soft aggregates in aqueous solution, spherical or filamentous in shape, at the critical micellar concentration (CMC) [33–35], and, due to their biodegradable, renewable, and eco-friendly nature, have been used in numerous environmental applications, for soil or wastewater remediation, without producing of secondary pollution [35–43]. As far as we know, the synthesis of porous/mesoporous silica in the presence of saponin as a template agent is poorly explored [44]. The aim of this research was to obtain two novel silica adsorbents, one which is a biosorbent, SiO_2@Saponin, the as-synthesized silica in the biosurfactant template method, and the second, wormlike mesoporous silica, meso-SiO_2, obtained by the removal of the saponin biosurfactant from pores by calcination of SiO_2@Saponin. Discontinuous experiments were carried out to assess the adsorption performance of the prepared silicas of Pb(II) and Cd(II) ions from single/binary solutions.

2. Materials and Methods

2.1. Reagents and Equipment

Weiss rein saponin from Merck ('saponin white'), tetraethoxysilane (TEOS), and HCl 36.5% (Sigma–Aldrich, Merck, Darmstadt, Germany) were used for the synthesis of silica. In

the adsorption experiments, stock solutions of metal ions with a concentration of 1000 mg/L were prepared using $Cd(NO_3)_2$ and $Pb(NO_3)_2$ from Merck, Darmstadt, Germany. HNO_3 10^{-3} mmol/L has been added to Pb(II)/Cd(II) stock solutions to adjust the solution's pH at a value lower than the precipitation pH. These solutions were diluted to prepare 100 mg/L, 75 mg/L, 50 mg/L, 25 mg/L, 10 mg/L and 5 mg/L concentration solutions. HNO_3 10^{-3} mmol/L and NH_4OH 10^{-4} mmol/L (analytical purity) were used to change the pH of metal ion solutions. Quantitative determination of Pb(II)/Cd(II) ions was performed using an AAnalyst 400 atomic absorption spectrometer manufactured by Perkin Elmer (Shelton, CT, USA), and pH was determined with an Agilent 3200P laboratory pH meter. Batch tests on the GFL 3031 Incubating Shaker (at 150 rpm) were carried out.

FTIR vibrational spectra of saponin, silica prepared in the presence of saponin (SiO_2@Saponin), and silica calcined at 550 °C for 6 h (meso-SiO_2) were recorded in the wavenumbers range of 4000–500 cm^{-1} with a Bruker Tensor 27 spectrophotometer, with the ATR sampling unit. Thermal analysis (TG-DSC) was performed with Netzsch 449C STA Jupiter equipment. The samples inserted in the Al_2O_3 crucible were heated at 10 °C/min up to 900 °C under dry synthetic air with a flow rate of 20 mL/min. An empty Al_2O_3 crucible was used as a reference. The silica samples were calcined in a Nabertherm HTC 03/16 furnace, T_{max}. 1600 °C. SEM images were recorded on an SEM/EDAX High-Resolution Scanning Electron Microscope, Quanta Inspect F50 (resolution 1.2 nm) with EDAX (133 eV resolution at MnKα)—FEI Company, Hillsboro, OR, USA. TEM/HRTEM images were recorded on a TECNAI F30 G2 high-resolution transmission electron microscope. This equipment operates at an accelerating voltage of 300-kV device. The samples have been ultrasonicated in methanol and subsequently collected into a holey carbon-coated TEM support grid. A Micromeritics ASAP 2020 analyzer (at −196 °C) has been used to record the N_2 adsorption/desorption isotherms. The samples were outgassed at 160 °C for at least 6 h under vacuum, and the specific surface areas (S_{BET}) were determined using the Brunauer–Emmett–Teller (BET) method. The pore size distribution curves were obtained using the Barrett–Joyner–Halenda (BJH) method based on the desorption branch. The total pore volume (V_{total}) was determined from the amount adsorbed at the relative pressure of 0.99.

2.2. Synthesis of SiO_2@Saponin and Meso-SiO_2

SiO_2@Saponin and meso-SiO_2 have been synthesized using the soft-template method for mesoporous silicas. The SiO_2 network has been formed in a sol–gel process with TEOS as a silica precursor templated by the micelles formed by the saponin biosurfactant. The saponin biosurfactant aqueous concentration was 8 mg/mL, which represents 4 times the CMC of saponin white (Merck & Co., Darmstadt, Germany) [45]. The saponin micelles were stabilized by maintaining the solution at pH = 2, with HCl 36.5%. For SiO_2@Saponin, a mixture consisting of saponin solution (8 mg/mL) and TEOS (added dropwise, under continuous stirring) in a 1:50 molar ratio was prepared and kept without stirring at room temperature for 16 h. The resulting silica gel was dried in an oven. To obtain the meso-SiO_2 material, a quantity of SiO_2@Saponin was calcined in air at 550 °C for 6 h to remove the saponin used as a structure-directing agent from the silica pores.

2.3. Adsorption Studies

The surfactant effect on the adsorption performance of silica prepared in the presence of saponin (SiO_2@Saponin) and silica calcined at 550 °C for 6 h (meso-SiO_2) was analyzed for Pb(II) and Cd(II) single-metal and binary-metals solutions, in batch tests. The observed parameters and tested conditions are shown in Table 1.

Table 1. Experimental conditions in adsorption tests.

Parameter	Experimental Conditions
Contact time 0–360 min	25 mL Pb(II)/Cd(II) 100 mg/L; 0.01 g adsorbent, room temperature
pH 2.5–7 pH units	25 mL Pb(II)/Cd(II) 100 mg/L; 0.01 g adsorbent; room temperature, 5 h contact time
Heavy metal ion concentration 5–100 mg/L	25 mL heavy metal ions solution; 0.01 g adsorbent; room temperature, 3/5 h contact time depending on the type of heavy metal ion

3. Results

3.1. Synthesis of SiO_2@Saponin and Meso-SiO_2

The saponin used in this work was the commercial Merck saponin white, a saponin isolated from the roots of *Gypsophila paniculata* [46]. This saponin, with the chemical formula $C_{30}H_{46}O_4$, belongs to the triterpenoid saponins with the aglycone moiety identified as gypsogenin and may have −OH and −COOH functional groups [34]. Saponin white forms small micelles (aggregates of 2–10 molecules formed above the CMC), rod-like, at critical micellar concentrations one or two orders of magnitude lower than that of ionic surfactants [43,45,47]. The micelles of saponin white are elongated, filamentous and they form in water at concentrations (CMCs): 1.4 mg/mL as reported by Böttcher [48] or 2.3 mg/mL CMC as determined by Korchowiec et al. [45]. Numerous studies stated that at pH = 2, the CMC is even lower than these values [49–51], and the H_3O^+ ions are adsorbed on the aggregate of saponin micelles, stabilizing them and, according to our objective, making them more prone to interact with silica precursor to form the silica network around them. The size and the micelle structure of saponin white were not clarified in detail, but the meso-SiO_2 obtained in the template synthesis and calcined at 550 °C have a wormlike porous structure, as TEM/HRTEM images revealed.

Both silicas, SiO_2@Saponin, and meso-SiO_2, have been assessed in sorption experiments to determine their adsorption capacities toward Pb(II) and Cd(II) ions from aqueous effluents. SiO_2@Saponin is a biosorbent with free carboxyl and hydroxyl moieties that can serve as ligands in coordinating the metallic ions, and the presence of these functional groups proved to be a key feature in the remediation of wastewater or contaminated soil [40,42].

3.2. Adsorbents Characterization

3.2.1. FTIR Spectra

FTIR spectra recorded for saponin, SiO_2@Saponin, and meso-SiO_2 are presented in Figure 1. In these FTIR spectra, stretching vibration bands ($\nu_{CH2as/sym}$, $\nu_{Si\text{-}O\text{-}Si}$, $\nu_{C\text{-}H}$, $\nu_{C=O}$, $\nu_{C\text{-}O\text{-}C}$) specific to silica network and organic moieties of the saponin surfactant are present. The spectrum of saponin shows specific bands: one at 3336 cm^{-1} for hydroxyl groups (-OH) and another one with a maximum at 2932 cm^{-1} that includes the symmetric and asymmetric stretching vibrations of the -CH_2- bonds. In the spectrum, there are also maxima at 1728 cm^{-1} for the stretch of the carbonyl bond (-CH=O) and at 1611 cm^{-1} for the stretching vibration of double bonds (-C=C-). The infrared bands at 1371/1251 cm^{-1} were attributed to C-O-C in ester moieties, and an intense absorption maximum was observed at ~1041 cm^{-1} to oligosaccharide linkages (C-O-C) [52].

In the FTIR spectrum of SiO_2@Saponin, the presence of saponin inside the material is confirmed by the presence of the broad absorption maximum centered at 1634 cm^{-1}; this also includes the peak from 1734 cm^{-1} (corresponding to -CH=O bond), the band is widened, probably due to the confinement effects, and the vibration of this bond is no longer observed as a distinct signal. The very broad band at 3359 cm^{-1}, shifted from 3336 cm^{-1} in the saponin spectrum, is ascribed to the overlapping of the stretching vibrations of hydroxyl (-OH) and silanol (-Si-OH) bonds [38]. The strongest signals in FTIR spectra at ~1051 cm^{-1} of both SiO_2@Saponin and meso-SiO_2 are ascribed to asymmetric vibration of

Si-O-Si, characteristic peaks confirming the formation of the silica network [53]. Also, the symmetric vibration mode of the SiO_2 group is present at 802 cm^{-1} in SiO_2@Saponin and meso-SiO_2 spectra [53]. For SiO_2@Saponin, the weak peak at 967 cm^{-1} was assigned to non-condensed Si-OH groups [53].

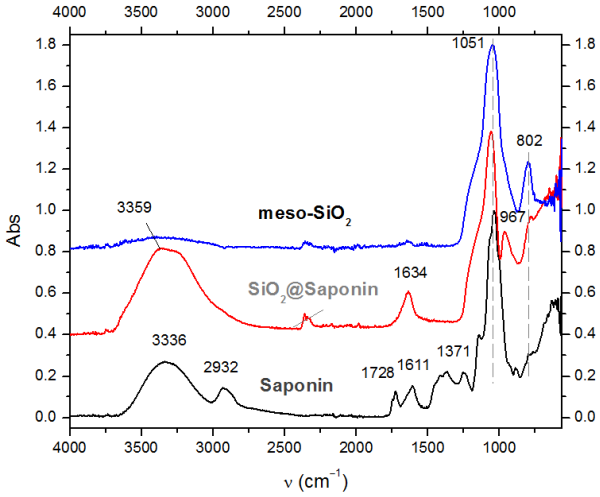

Figure 1. FTIR spectra of Saponin, SiO_2@Saponin, and meso-SiO_2 (the spectra were normalized and shifted on the y-axis).

After thermal treatment (calcination), the saponin surfactant from the silica pores is removed, and the characteristic maxima of saponin are no longer present in the IR spectrum of meso-SiO_2 (Figure 1).

3.2.2. Thermal Analysis (TG-DSC)

TG-DSC analyses (Figure 2, Table 2) support the conclusion of spectroscopic analysis, namely that the silica network was formed by the incorporation of saponin micelles, the mass loss being larger in the case of SiO_2@Saponin (~10.3–10.5%), suggesting the loading of organic compound into synthesized silica. Weak endothermic effects (T_1) take place between 25 and 150 °C and can be attributed to the loss of water. The TG curve of saponin shows a significant mass loss (55.27%) accompanied by two thermal effects at T_2 = 330 °C and T_3 = 483.8 °C, followed by another decomposition step, T_4 = 586.5 °C, with 34.18% mass loss. At 800 °C, the saponin loses about 98.1% of its mass (Figure 2a, Table 2). These steps, corresponding to the combustion of organic matter, are characterized by strong exothermic effects (Figure 2b).

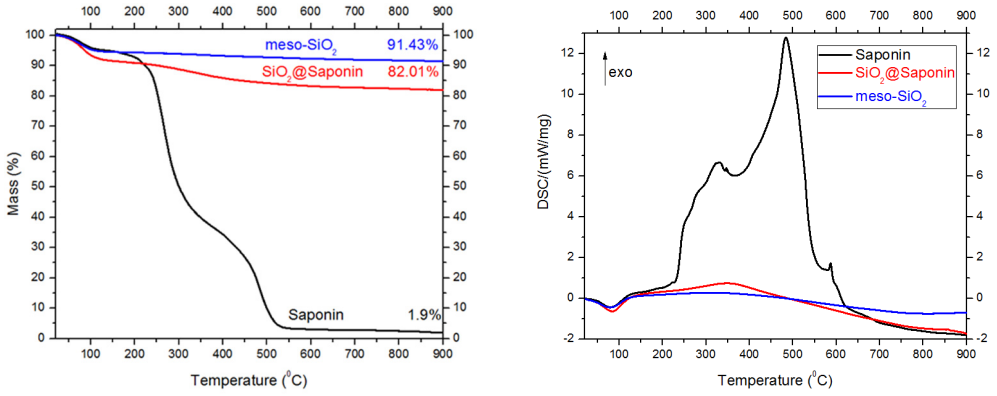

Figure 2. (**a**) TG and (**b**) DSC curves for Saponin, SiO_2@Saponin, and meso-SiO_2.

Table 2. Thermal effects, maximum temperature/effect, and corresponding mass loss.

Compound	T_1 (°C)	Δm_1 (%wt)	T_2 (°C)	T_3 (°C)	Δm_2 (%wt)	T_4 (°C)	Δm_3 (%wt)	Residual Mass (%wt)	Δm (%wt)
Saponin	80.8	7.23	330.9	483.8	55.27	586.5	34.18	1.9	98.1
SiO_2@Saponin	84.5	8.45	349.4	–	8.29	–	–	82.01	17.99
meso-SiO_2	79.2	5.51	318.4	–	2.22	–	–	91.43	8.57

The SiO_2@Saponin thermal decomposition profile presents a small mass loss (8.45%) up to 150 °C, assigned to water/solvent removal, and another mass loss of 8.29%, observed from 150 to 600 °C, which corresponds to the decomposition/oxidation of saponin incorporated in silica, but also to the condensation of silanol Si-OH moieties on the surface of silica, and its densification (Figure 2a, Table 2). The mass loss is accompanied by a small exothermic effect. The reduced intensity of this effect can indicate a different decomposition/oxidation pathway of low intensity due to the slower oxygen diffusion and can also be explained by better thermal stability of saponin when included in silica (Figure 2b).

The TG curve of meso-SiO_2 indicates a small mass loss of about 8.57% over the whole temperature range, and this can be attributed to the thermal desorption of water (5.51% up to 150 °C) and the further dehydroxylation and condensation of silanol groups in the process of densification of the silica matrix. The higher mass loss in the case of SiO_2@Saponin suggests the incorporation of the biosurfactant in the pores of the formed silica network. The mass loss is much lower in the case of calcined SiO_2, meso-SiO_2 (2.22% at T_2 = 318.4 °C, in the combustion stage of the organic part), which corresponds to the fact that the saponin has been eliminated from the silica pores.

3.2.3. SEM/EDX Analysis

The surface and morphology of the two adsorbent materials, SiO_2@Saponin, and meso-SiO_2, are illustrated in Figure 3.

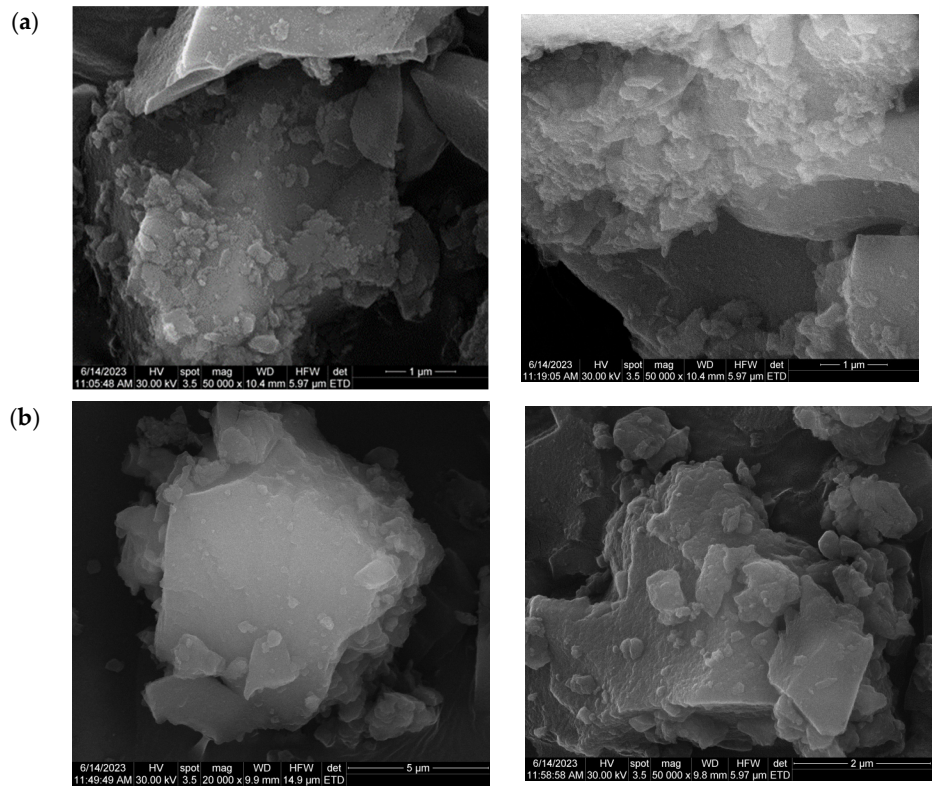

Figure 3. SEM images of (**a**) SiO_2@Saponin and (**b**) meso-SiO_2.

From the analysis of the SEM images, it is found that the materials are composed of non-uniform aggregates of relatively large particles with rigid lamellar structures. It can be estimated that the size of the aggregates is ~3–5 μm for the prepared silicas, and the shapes of the aggregates are very similar.

The SiO_2 network in SiO_2@Saponin has a layered morphology, which suggests the possibility of cleavage. In meso-SiO_2, the consistency of the platelets that form the aggregates seems to have changed, and the structure appears less dense (Figure 3b).

From the EDX patterns (Figure 4), one can observe that the adsorbent materials are pure. Only the elements Si, O, C (with the characteristic spectral lines) are present, with relative intensities that suggest a higher carbon (and oxygen) content in the case of SiO_2@Saponin (Si:O:C = 6.45:1.93:1) than in the case of meso-SiO_2(Si:O:C = 6.45:1.21:1.1).

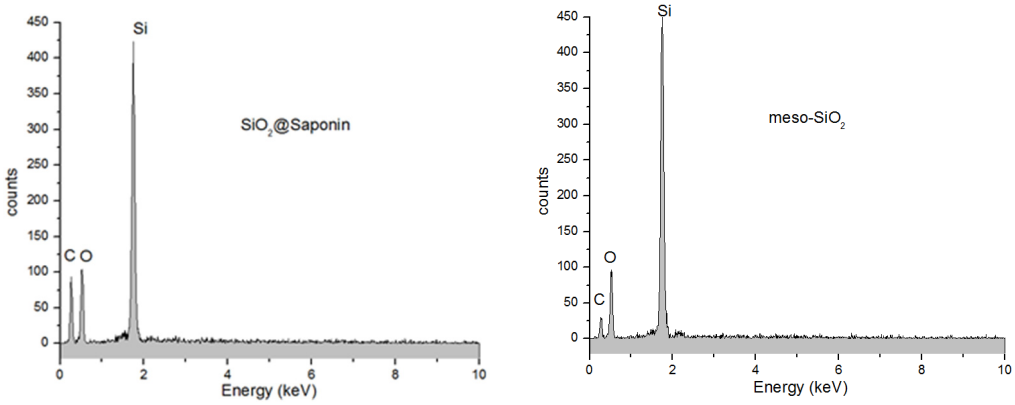

Figure 4. EDX patterns of SiO_2@Saponin and meso-SiO_2.

3.2.4. High-Resolution Transmission Electron Microscopy (HRTEM)

In addition to SEM analysis, TEM/HRTEM images (Figure 5), recorded at the same magnitude (×50,000) and resolution (20 nm) for both samples, confirm the porous structure of meso-SiO_2.

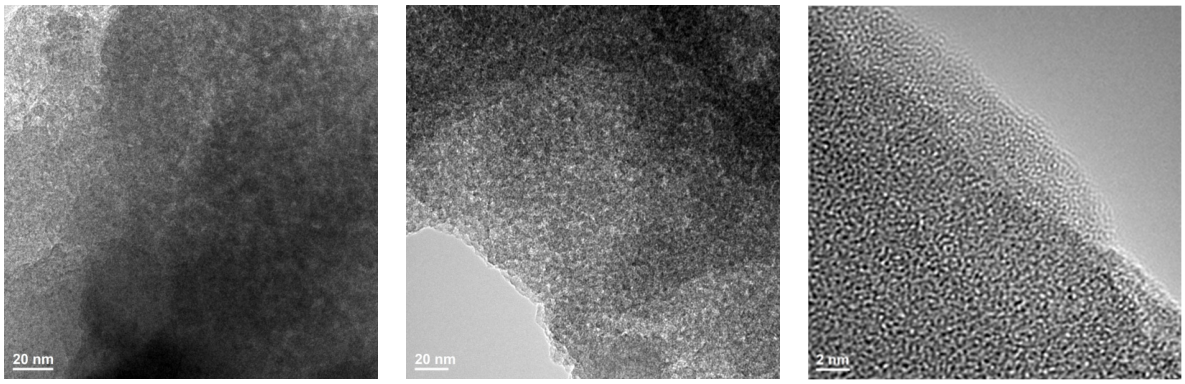

(**a**) (**b**) (**c**)

Figure 5. HRTEM images (20 nm) of (**a**) SiO_2@Saponin and (**b**) meso-SiO_2; (**c**) HRTEM image (2 nm) of meso-SiO_2.

SiO_2@Saponin has a denser structure, while meso-SiO_2 has a wormlike mesoporous structure with apparently uniformly distributed mesopores. This morphology is easier to observe at the HRTEM resolution of 2 nm (Figure 5c) and can be explained by the existence of micellar self-assembly of saponin and by the elongated nature of the micelles.

3.2.5. Nitrogen Adsorption–Desorption Isotherms

The surface area and porosity of the synthesized SiO_2@Saponin and meso-SiO_2 silicas were estimated using the N_2 gas adsorption method at −196 °C. The N_2 adsorption–desorption isotherms of both samples (Figure 6) are type IV according to IUPAC classification, with H2(a)-type hysteresis [54]. This is indicative of capillary condensation phenomena within mesoporous structures. The H2(a)-type hysteresis loops suggest the existence of complex pore networks with interconnected pores. This type of hysteresis loop can arise from pore-blocking-induced percolation effects in pore networks, where the liquid in the pore cavities evaporates as the largest neck evaporates [55]. The inset plots of Figure 6 illustrate the pore size distribution (PSD) of the samples. As can be seen, the PSD is narrow in both samples, with the average pore width having close values and slightly higher in the case of meso-SiO_2 (Table 3). It is worth mentioning that the peak maximum for the meso-SiO_2 sample has a higher value (3.9 nm) than for SiO_2@Saponin (3.6 nm). This suggests that the removal of saponin, the silica structure-directing agent, led to the collapse of micropores and smallest mesopores and, hence, to a decrease in the surface area and porosity of the meso-SiO_2 sample (Table 3). However, the ordered mesoporous structure was preserved, as demonstrated by HRTEM images.

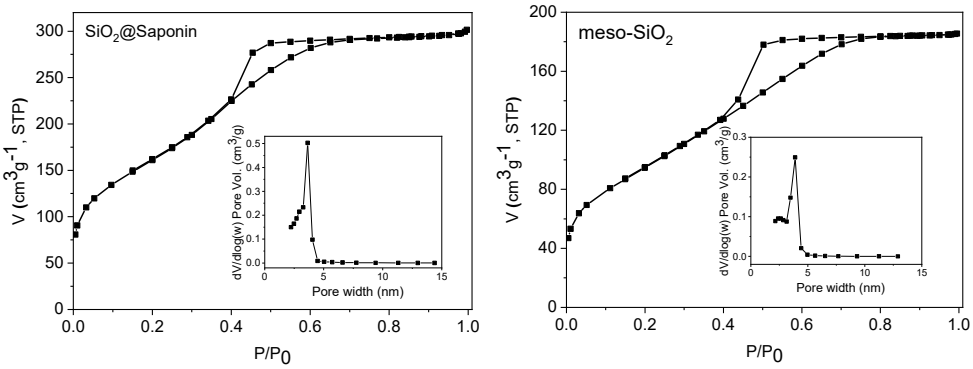

Figure 6. Nitrogen adsorption–desorption isotherms of SiO_2@Saponin and meso-SiO_2.

Table 3. Textural properties of SiO_2@Saponin and meso-SiO_2.

Sample	S_{BET} (m^2/g)	Pore Volume (cm^3/g)	d * (nm)
SiO_2@Saponin	587.5	0.466	3.28
meso-SiO_2	347.2	0.286	3.32

* d = BJH desorption average pore width.

3.3. Adsorption Studies

To highlight the effect of the surfactant (saponin) on the adsorption capacity of the silica for Pb(II) and Cd(II) ions, batch tests were performed on the sorption of Pb(II)/Cd(II) ions in single-metal and binary solutions. In these tests, SiO_2@Saponin and meso-SiO_2 were used as adsorbents.

3.3.1. pH Effect

The pH appreciably influences the adsorption capacity of the materials since it determines the type of ionic species in the form of which metal ions are found in aqueous solutions, and the electrical charges of the functional groups grafted onto the structure of the adsorbents. The results regarding the effect of pH on the adsorption capacity of Pb(II)/Cd(II) onto SiO_2@Saponin and meso-SiO_2 are presented in Figure 7.

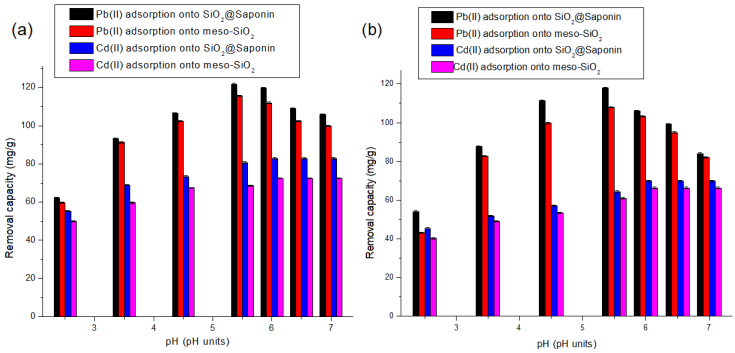

Figure 7. The pH effect on Pb(II)/Cd(II) adsorption onto SiO_2@Saponin and meso-SiO_2 from single (**a**) and binary solutions (**b**).

The data presented in Figure 7 reveal that reduced pH values have resulted in low adsorption capacity values. This behavior is determined by the existence of a competitive effect between protons in the solution and Pb(II)/Cd(II) ions to occupy the free active groups on the adsorbent's surface (SiO_2@Saponin/meso-SiO_2). As the pH increases, the concentration of protons in the aqueous effluent decreases, and, as a result, the retention capacity of SiO_2@Saponin/meso-SiO_2 increases. In the case of the Pb(II) ion, an optimal pH value of 5.5 was established, and for Cd(II) ions, an optimal pH value of 6 was experimentally determined. After reaching the optimum pH value, a slight decrease in the retention capacity of Pb(II) ions was observed, and in the case of Cd(II) ions, the retention capacity value is constant at pH values higher than 6. It can be appreciated that when hydrolyzed species appear in solution, nanometric precipitates, in our case, cover the "active" surface available for Pb(II) ions adsorption. The results are consistent with those found by Sumanjeet et al. [56], Verma et al. [57], and Ifijen et al. [58]. Sajid et al. observed the coating of sorbent with metal hydroxides and an increase in the time for sample filtration [59]. This behavior was noticed both in the retention process of Pb(II)/Cd(II) ions from single aqueous effluents and from binary solutions. A decrease in the retention capacity characteristic of both metal ions was observed for binary effluents due to the competitive effect of each of them in occupying the free active centers. Similar results were found by Lian et al. [60], who have reported that onto ragweed biochar and horseweed biochar at pH 5.5, in a binary system, the adsorption capacity is >95.10% for Cd(II) and >95.20% for Pb(II).

Taking into account these results, experiments were performed to establish the effect of other parameters at the optimum pH values mentioned above.

The greater adsorption capacity of SiO_2@Saponin is due, on the one hand, to the saponin present in the silica pores. The carboxyl and hydroxyl functional groups of saponin are involved in the interaction with Pb(II) and Cd(II) ions and, on the other hand, in its large specific surface area.

3.3.2. The Contact Time Effect

When the experiments from the laboratory level need to be upscaled at the pilot scale, it is necessary to establish the optimum time to reach the equilibrium. The obtained experimental results are shown in Figure 8.

As can be observed from Figure 8, the retention process of Pb(II) and Cd(II) ions from single/binary solutions on SiO_2@Saponin/meso-SiO_2 can be described as a two-step process. A fast step that takes place in the first 60 min for both metal ions removed was observed. This was followed by a slower step that takes place between 60 and 240/300 min, depending on the nature of the metal ion. The explanation for this behavior is that in the first 30 min, there is a high density of free functional groups involved in the binding of metal ions, then the number of free functional groups decreases, and as a result, the increase in retention capacity is slower. This behavior is valid for both metal ions.

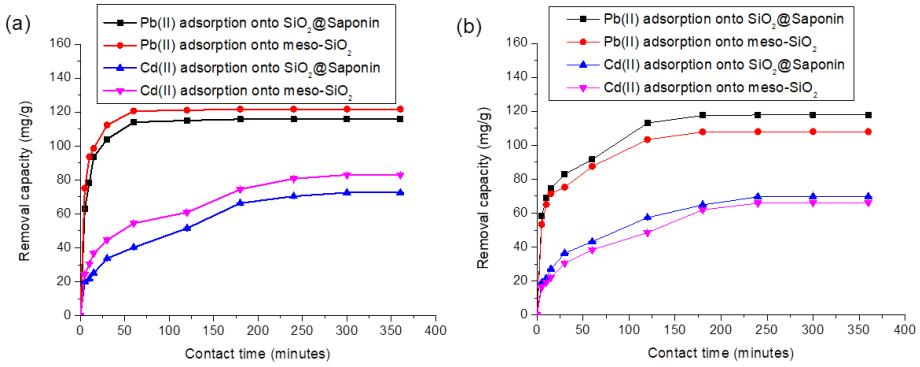

Figure 8. The contact time effect on Pb(II)/Cd(II) adsorption onto SiO_2@Saponin and meso-SiO_2 from single (**a**) and binary solutions (**b**).

Another observation is that, for the Pb(II) ion, the time required to reach the equilibrium is approximately three hours, and for the Cd(II) ion, the time to reach the equilibrium is five hours. This observation determined that the experiments performed to assess the retention of Pb(II) ions were to be carried out for three hours, and those on the retention of Cd(II) ions for five hours.

It can also be noted that the retention capacity of Pb(II) ions determined experimentally is 121.76 ± 0.45 mg/g in the case of the SiO_2@Saponin sample and 115.89 ± 0.34 mg/g in the case of the sample meso-SiO_2, while the Cd(II) ion retention capacity determined experimentally is 82.97 ± 0.31 mg/g in the case of the SiO_2@Saponin sample and 72.5 ± 0.25 mg/g in the case of the meso-SiO_2 sample.

The higher value of the retention capacity of Pb(II) ions compared to the value of the retention capacity of Cd(II) ions is caused by its characteristics. Thus, according to literature data, ions with larger radii are much more easily retained by adsorbents [61]. As a result, the larger value of the radius of the Pb(II) ions (1.20 Å) compared to 0.95 Å—the value of the radius of the Cd(II) ions [62] determined that the prepared silica samples presented a higher retention of Pb(II) ions. This can also be correlated with the stability of hydrated metal ions (aqua ions). Metal ions with smaller radii present higher hydration energies and are stabilized in aqueous solutions, and consequently, adsorption becomes difficult [61]. The hydrated Pb(II) ion has a radius of 4.01 Å and the hydrated Cd(II) ion of 4.26 Å, and the lower value of the radius of hydrated species of Pb(II) determined the higher value of the retention capacity for Pb(II) ions [61].

Another factor that influences the retention capacity is the electronegativity of the metal ion. Metals with higher electronegativity are retained much more easily than metals with lower electronegativity. Therefore, the value of the electronegativity of Pb(II) ions (2.33) higher than of Cd(II) ions (1.69) can also explain the greater retention capacity of Pb(II) ions compared to Cd(II) ions [62].

3.3.3. Adsorption Isotherm

In industrial adsorption processes, it is relevant to know the equilibrium data, the maximum adsorption capacity, and the adsorption kinetics for design and optimization. The most intensively applied isotherm models for the characterization of adsorption processes are the Freundlich and Langmuir isotherm models.

The Freundlich isotherm is applicable in adsorption studies on rough and multisite (heterogeneous) surfaces [63]. The mathematical model of the Freundlich isotherm is presented in Table 4.

The Langmuir isotherm model (Table 4) is applied to characterize the adsorption processes on homogeneous surfaces. Another hypothesis of this isotherm model is the reversibility of the adsorption–desorption process [64].

Table 4. The mathematical expression of the isotherm models used to model the Pb(II)/Cd(II) adsorption from single/binary solutions.

Isotherm	Mathematical Expression	Plot
Nonlinear Freundlich	$Q_e = K_F \times C_e^{\frac{1}{n}}$	Q_e vs. C_e
Nonlinear Langmuir	$Q_e = \frac{Q_{max} K_L C_e}{1+K_L C_e}$	Q_e vs. C_e
Linear modified Langmuir for heavy metal 1	$\frac{1}{Q_{e,M1}} = \frac{1}{Q_{max,M1}} + \frac{1}{Q_{max,M1} K_{L,M1}} \left[\frac{1}{C_{e,M1}} + \frac{K_{L,M2} C_{e,M2}}{C_{e,M1}}\right]$	$\frac{1}{Q_{e,M1}}$ vs. $\left[\frac{1}{C_{e,M1}} + \frac{K_{L,M2} C_{e,M2}}{C_{e,M1}}\right]$
Linear modified Langmuir for heavy metal 2	$\frac{1}{Q_{e,M2}} = \frac{1}{Q_{max,M2}} + \frac{1}{Q_{max,M2} K_{L,M2}} \left[\frac{1}{C_{e,M2}} + \frac{K_{L,M1} C_{e,M1}}{C_{e,M2}}\right]$	$\frac{1}{Q_{e,M2}}$ vs. $\left[\frac{1}{C_{e,M2}} + \frac{K_{L,M1} C_{e,M1}}{C_{e,M2}}\right]$

The adsorption capacity and selectivity of an adsorbent towards a certain metal ion as a pollutant is influenced by numerous factors, which are grouped into the following: (1) characteristics of the adsorbent material: specific surface area, porosity, types, and the number of functional groups; (2) the characteristics of metal ions: hydrated ion radius, ionic radius, hydration enthalpy, electronegativity and (3) the characteristics of the solution such as concentration, pH, and the presence of competing ions.

The competitive adsorption of pollutants (metal ions/organic pollutants/other inorganic pollutants) from binary solutions can be characterized by applying the modified Langmuir isotherm equation introduced originally by Weber and Digiano (Table 4) [64–67].

In the Freundlich isotherm, Q_e is the adsorption capacity at equilibrium (mg/g), C_e represents the equilibrium concentration (mg/L), K_F ((mg/g)(L/mg)$^{1/n}$), and n are the adsorption potential and the adsorption intensity constant [63]. The values of n in the Freundlich isotherm equation and the values of the n parameter describe the heterogeneity of a surface. Homogeneous surfaces are considered to have n = 1, which indicates that the adsorption capacity is proportional to the percentage of occupied/occupied sites/centers [63].

In the Langmuir isotherm, C_e describes the equilibrium concentration of metal ions (mg/L), K_L represents the equilibrium constant of the Langmuir model that defines the adsorption energy (L/mg), Q_e represents the adsorption capacity at equilibrium (mg/g), Q_{max} is the maximum adsorption capacity determined from the Langmuir isotherm (mg/g) [64].

The parameters of linear modified Langmuir for heavy metals ($M1$, $M2$) equations are defined as follows:

- $C_{e,M1}$, $C_{e,M2}$, $Q_{e,M1}$, and $Q_{e,M2}$ represent the equilibrium concentrations and equilibrium retention capacity of metal ions ($M1$) (Pb(II)) and ($M2$) (Cd(II)) in binary solutions;
- $K_{L,M1}$ and $K_{L,M2}$ represent the characteristic equilibrium constants for the adsorption of the respective metal ions from single solutions;
- $Q_{max,M1}$ and $Q_{max,M2}$ represent the maximum adsorption capacities for the experiments with metal ions from the binary solutions.

To determine the values of $Q_{max,M1}$ and $Q_{max,M2}$, linear modified Langmuir for heavy metals ($M1$, $M2$) equations will be represented graphically. The linear representation $\frac{1}{Q_{e,M1}}$ vs. $\left[\frac{1}{C_{e,M1}} + \frac{K_{L,M2} C_{e,M2}}{C_{e,M1}}\right]$ will be used to determine $Q_{max,M1}$ and the linear representation $\frac{1}{Q_{e,M2}}$ vs. $\left[\frac{1}{C_{e,M2}} + \frac{K_{L,M1} C_{e,M1}}{C_{e,M2}}\right]$ will be used to calculate $Q_{max,M2}$.

To establish the dynamics of the adsorption process of Pb(II) and Cd(II) ions from binary solutions onto SiO_2@Saponin/meso-SiO_2, the ratio $\frac{Q_{max,binary}}{Q_{max,single}}$ will be calculated [62].

The effects that each of the two metal ions can have on each other are:

- synergistic effects when the value of the ratio $\frac{Q_{max,binary}}{Q_{max,single}}$ is above unity, and the effect of the mixture is stronger than the effect of individual metal ions;
- antagonistic effects if the ratio $\frac{Q_{max,binary}}{Q_{max,single}}$ is below 1, the two metal ions have an antagonistic effect, and the mixture has a weaker effect compared to the effect of the individual metal ions;

- the mixture has no effect on the adsorption process of metal ions from binary solutions if the ratio $\frac{Q_{max,binary}}{Q_{max,single}}$ is equal to 1 [68].

From the graphical representations (Figures 9 and 10) of the experimental results, the parameters of the nonlinear adsorption isotherms for the adsorption of Pb(II)/Cd(II) ions on SiO_2@Saponin/meso-SiO_2 were determined (Table 5).

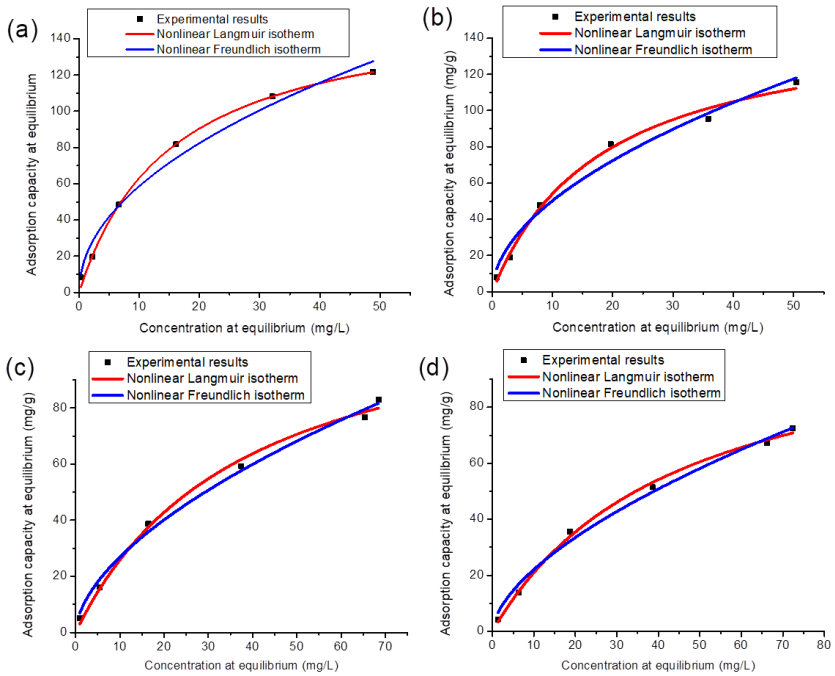

Figure 9. Nonlinear Langmuir and Freundlich isotherms for Pb(II) adsorption onto SiO_2@Saponin (**a**), meso-SiO_2 (**b**), and Cd(II) adsorption onto SiO_2@Saponin (**c**), meso-SiO_2 (**d**), from single solutions.

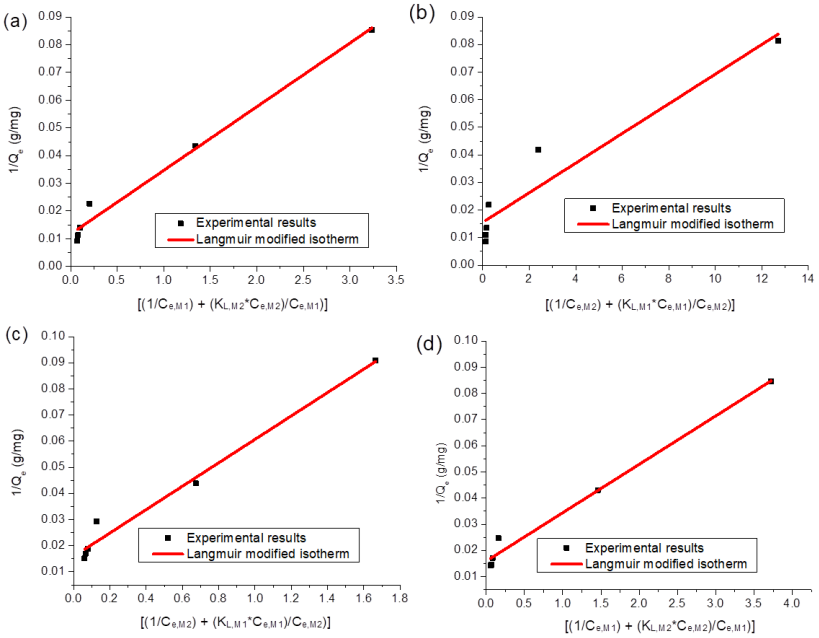

Figure 10. Langmuir modified isotherm for Pb(II) adsorption onto SiO_2@Saponin (**a**), meso-SiO_2 (**b**), and Cd(II) adsorption onto SiO_2@Saponin (**c**), meso-SiO_2 (**d**) from binary solutions.

Table 5. Langmuir and Freundlich isotherm parameters for the adsorption process of Pb(II)/Cd(II) ions from single solutions on SiO_2@Saponin and meso-SiO_2.

Adsorbent	**SiO_2@Saponin**	**Meso-SiO_2**	**Adsorbent**	**SiO_2@Saponin**	**Meso-SiO_2**
Heavy metal ion	Pb(II)		Heavy metal ion	Cd(II)	
Langmuir parameters					
Q_{max} (mg/g)	159.6	152.9	Q_{max} (mg/g)	124.5	114.1
K_L (L/mg)	0.0654	0.0547	K_L (L/mg)	0.0262	0.0226
R^2	0.9965	0.9915	R^2	0.9939	0.9965
R_L	0.1326	0.1259	R_L	0.2762	0.3067
AIC	27.74	32.19	AIC	26.52	21.66
Freundlich parameters					
K_F $((mg/g)(L/mg)^{1/n})$	18.99	14.91	K_F $((mg/g)(L/mg)^{1/n})$	7.123	5.524
1/n	0.4899	0.5277	1/n	0.5773	0.6016
R^2	0.9748	0.9742	R^2	0.9922	0.9897
AIC	38.67	38.81	AIC	28.02	28.08

The correlation coefficient (R^2) was used to determine the isotherm model that characterizes the studied adsorption process. An R^2 parameter value close to 1 suggests the fit of the tested model with the studied adsorption process.

The separation factor (R_L), calculated with the formula: $R_L = \frac{1}{1+K_L C_0}$, where C_0 (mg/L) defines the initial concentration of Pb(II)/Cd(II) ions, and K_L is the Langmuir equilibrium constant represents another parameter that shows the correlation of the experimental results of the studied adsorption process with the Langmuir isotherm model. According to the literature data, the R_L parameter with values between 0 and 1 indicates that the studied adsorption is favorable, while $R_L > 1$ adsorption is not favorable, and $R_L = 1$ indicates a linear process [69]. In the experimental tests carried out, the values of R_L are between 0 and 1, which indicates the favorability of the studied adsorption process. A higher adsorption capacity reflects a high specific surface and high pore volume of the adsorbent.

Another indicator used to determine which of the two models characterizes an adsorption process is the Akaike Information Criterion (AIC) parameter. Lower AIC values suggest that the analyzed model is valid for defining the studied adsorption [69].

Assessment of all the isotherm model parameters concluded that the Langmuir isotherm model fits better with the Pb(II)/Cd(II) adsorption process onto SiO_2@Saponin and meso-SiO_2. Thus, the adsorption of Pb(II)/Cd(II) adsorption onto SiO_2@Saponin and meso-SiO_2 takes place as monolayer adsorption onto a homogeneous surface [69]. The competitive adsorption of the experimental results has been modeled using the equations from Table 4. The values of equilibrium constant $K_{L,M1}$ and $K_{L,M2}$ have been determined for the Langmuir linear isotherm of the respective metal ions from single solutions.

The graphical representations used to determine the maximum values of the removal adsorption capacities for Pb(II) and Cd(II) ions in binary solutions from the modified Langmuir isotherm are shown in Figures 10 and S1.

Table 6 shows the maximum retention capacity values for Pb(II) and Cd(II) ions determined from the modified Langmuir isotherm and the $\frac{Q_{max,binary}}{Q_{max,single}}$ ratio values for the SiO_2@Saponin and meso-SiO_2 samples.

Table 6. Maximum values of the removal capacity of Pb(II) and Cd(II) ions determined from the Langmuir isotherm for single and binary solutions.

Adsorbent	Heavy Metal Ion	Q_{max} (Single Solution) (mg/g)	Q_{max} (Binary Solution) (mg/g)	$\frac{Q_{max,binary}}{Q_{max,single}}$
SiO_2@Saponin	Pb(II)	159.6	94.51	0.5919
	Cd(II)	124.5	75.22	0.6040
meso-SiO_2	Pb(II)	152.9	85.47	0.5587
	Cd(II)	114.1	62.89	0.5484

The results presented in Table 6 indicate the following:

- both for the SiO_2@Saponin and for the meso-SiO_2, the values of the ratio $\frac{Q_{max,binary}}{Q_{max,single}}$ are lower than 1, which reveals that the adsorption of Pb(II) ions is hindered by the adsorption of Cd(II) and vice versa (both metal ions show a competition effect);
- both for the Pb(II) ion and the Cd(II) ion, there is a decrease in the maximum retention capacity determined from the linearized Langmuir isotherm in the retention process from binary solutions compared to the retention from single solutions;
- the higher values of the retention capacity of Pb(II) ions are explained based on the properties of the previously retained Pb(II) ions;
- it was also observed that in the case of meso-SiO_2, Pb(II) has a more intense effect on the Cd(II) removal from binary solutions, and in the case of SiO_2@Saponinthe stronger effect has been manifested by the Cd(II) ions.

3.3.4. Kinetic Study

Adsorption kinetics defines the rate of solute adsorption, and obviously, this rate governs the residence time of adsorbate retention at the solid-solution interface. Experimental data on adsorption kinetics were analyzed using three types of adsorption kinetics often used for this purpose. These are pseudo-first-order kinetics, pseudo-second-order kinetics, and intraparticle diffusion. The mathematical expressions of the kinetic models used to model the experimental results are described in Table 7.

Table 7. The mathematical expression of the kinetic models used to model the Pb(II)/Cd(II) adsorption from single solutions.

Kinetic Model	Mathematical Expression	Plot
Pseudo-first-order	$Q_t = Q_e(1 - exp(-k_1 t))$	Q_t vs. time
Pseudo-second-order	$Q_t = \frac{t}{\left(\frac{1}{k_2 Q_e^2}\right) + \left(\frac{t}{Q_e}\right)}$	Q_t vs. time
Intraparticle diffusion (IPD)	$Q_t = k_i t^{1/2} + C$	Q_t vs. time$^{1/2}$

The parameters included in Table 7 are described as follows: Q_e (mg/g) is the adsorption capacity of Pb(II)/Cd(II) at equilibrium, Q_t (mg/g) represents the adsorption capacity of Pb(II)/Cd(II) at time t (min), k_1 (min^{-1}) is the rate constant of pseudo-first-order, k_2 (mg/g·min) represents the second-order rate constant, k_i defines the intraparticle diffusion rate constant (mg/g·min$^{1/2}$), and C (mg/g) is the intersection representing the boundary layer thickness [69].

The kinetic parameters of the kinetic models tested and the correlation coefficient R^2 were determined from the graphic representation of the adsorption capacity as a function of t.

To calculate the kinetic parameters of the studied models, the results from Figure 11 have been used. The values obtained for these parameters are depicted in Table 8.

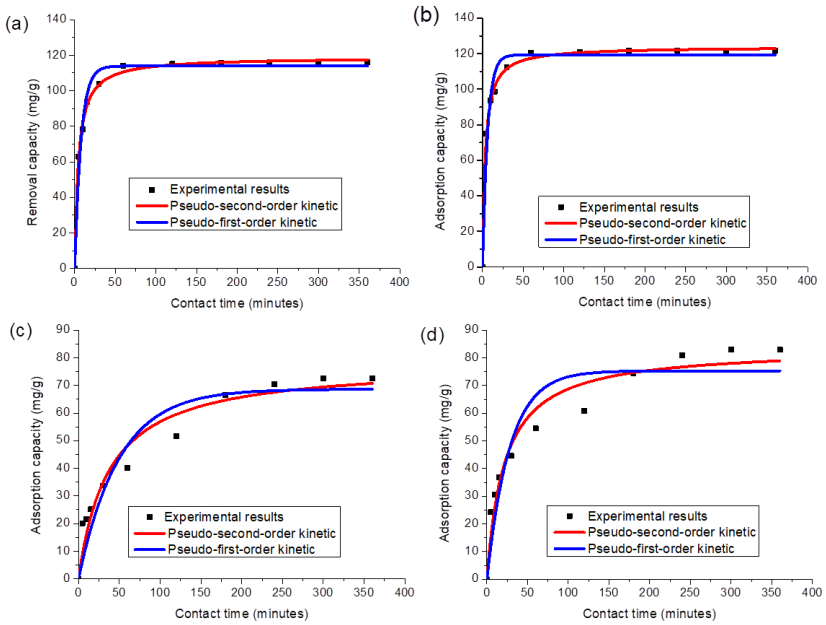

Figure 11. The graphical representations of the pseudo-first-order and pseudo-second-order kinetic models for the adsorption process of Pb(II) on SiO_2@Saponin (**a**) and meso-SiO_2 (**b**), Cd(II) on SiO_2@Saponin (**c**) and meso-SiO_2 (**d**).

Table 8. Kinetic parameters for Pb(II) and Cd(II) adsorption onto SiO_2@Saponin and meso-SiO_2 (nonlinear regression) from single aqueous solutions.

Adsorbent	SiO_2@Saponin	Meso-SiO_2
	Pb(II)	
Q_{exp} (mg/g)	121.7	115.8
Pseudo-first-order kinetic model		
Q_{calc} (mg/g)	119.3 ± 1.982	113.9 ± 1.738
k_1 (min^{-1})	0.1622 ± 0.0151	0.1282 ± 0.0099
R^2 adjusted	0.9796	0.9842
Pseudo-second-order kinetic model		
Q_{calc} (mg/g)	123.9 ± 0.6681	118.8 ± 0.8907
$k_2 \cdot 10^{-4}$ (g/mg·min)	24.3 ± 1.1382	18.6 ± 1.0691
R^2 adjusted	0.9983	0.9970
	Cd(II)	
Q_{exp} (mg/g)	82.97	72.50
Pseudo-first-order kinetic model		
Q_{calc} (mg/g)	75.30 ± 4.063	68.64 ± 4.043
k_1 (min^{-1})	0.0355 ± 0.0079	0.0202 ± 0.0046
R^2 adjusted	0.8920	0.9051
Pseudo-second-order kinetic model		
Q_{calc} (mg/g)	83.66 ± 3.750	78.04 ± 4.621
$k_2 \cdot 10^{-4}$ (g/mg·min)	5.512 ± 1.299	3.433 ± 0.9730
R^2 adjusted	0.9528	0.9471

Analyzing the data in the table above, the following can be concluded: the correlation coefficient R^2 is the closest to 1 for the second-order pseudo-kinetic model; for both metal ions, the experimental value of the adsorption capacity comes closest to the value of the capacity calculated from the kinetic model for the second-order pseudo-kinetic model; according to the second-order pseudo-kinetic model, the adsorption process of Cd(II) and Pb(II) ions on SiO_2@Saponin and meso-SiO_2 proceeds through chemical reactions [62].

A two-phase process comprises one first phase—external mass transfer and the second phase—intraparticle diffusion, which is used to describe the adsorption of heavy metal ions [70]. As with other adsorption processes, the removal kinetics is mainly related to the movement of Pb(II) and Cd(II) ions from the aqueous effluent towards the SiO_2@Saponin and meso-SiO_2 surfaces. The Weber-Morris intraparticle diffusion model (IPD) (equation 3) from Table 7 is applied to define this movement [70]. In the case of this kinetic model, if the straight line generated by the plot Q_t vs. time$^{1/2}$ is passing through the origin, it can be stated that intraparticle diffusion can be employed/used to describe the adsorption mechanism [70]. The slope of the linear curve defines the rate constant of the intraparticle diffusion process. The kinetic data of the adsorption processes studied were analyzed using the IPD model (Figure 12).

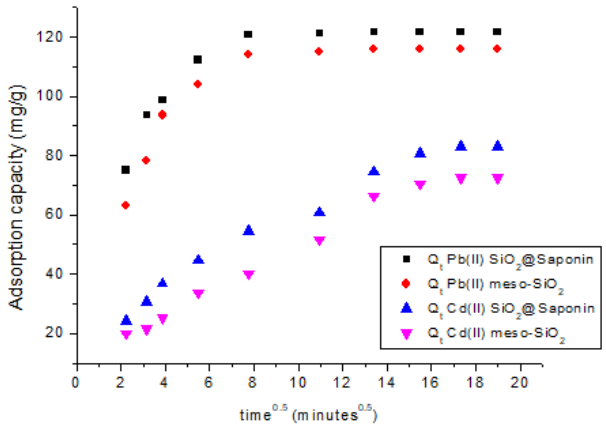

Figure 12. The graphical representations of the intraparticle diffusion kinetic model for the adsorption process of Pb(II) and Cd(II) from single-component solutions on SiO_2@Saponin and meso-SiO_2.

This figure reveals that the plot Q_t versus time$^{1/2}$ failed to pass through the origin. Moreover, the plots are divided into two or more segments, suggesting that intraparticle diffusion is not the only rate-limiting step. Similar results are also presented in the literature data [70].

3.3.5. Comparison of the Adsorption Capacity of SiO_2@Saponin and Meso-SiO_2 with Other SiO_2 Based Materials

The adsorption capacity of the as-prepared adsorbents compared to other SiO_2-based adsorbents is significant from a practical viewpoint. The results of this research were compared to literature data, and the maximum removal capacity (Q_{max}) specific for Cd(II) and Pb(II) are shown in Table 9.

As listed in Table 9, the SiO_2@Saponin and meso-SiO_2 samples investigated in this study are described by higher adsorption capacities than other SiO_2-related adsorbents (even if they are functionalized). It can also be observed from Table 9 that, in most cases, the Pb(II) and Cd(II) adsorption capacity of SiO_2@Saponin and meso-SiO_2 from binary solutions are higher than Pb(II) and Cd(II) adsorption capacity of other SiO_2 from single solutions. From the survey of articles that mention the removal of Pb(II) and Cd(II) ions by adsorption on SiO_2-based materials, only one paper reports results on the removal of the respective ions from multicomponent solutions.

Table 9. Pb(II) and Cd(II) adsorption capacity for different silica adsorbents.

Adsorbent	Pb(II) Adsorption Capacity (mg/g)	Cd(II) Adsorption Capacity (mg/g)	Refs
SiO_2 nanoparticles	34.2	42.2	[71]
MgO-SiO_2	102.02	94.05	[72]
Fe_3O_4@SiO_2-EDTA SiO_2: EDTA= 1:1 SiO_2: EDTA = 1.5:1 SiO_2: EDTA = 2:1 SiO_2: EDTA = 2.5:1 SiO_2: EDTA = 3:1	 74.07 79.37 86.21 114.94 101.01	 50.25 	[73]
SiO_2-EDTA	147.52		[74]
Fe_3O_4@SiO_2–NH_2	0.37 mmol/g at 25 °C 0.45 mmol/g at 35 °C 0.54 mmol/g at 45 °C	0.20 mmol/g at 25 °C 0.27 mmol/g at 35 °C 0.33 mmol/g at 45 °C	[75]
Fe_3O_4@SiO_2–NH_2-PAA	108.82	100.81	[76]
chitosan/SiO_2/Fe_3O_4 EDTA-modified chitosan/SiO_2/Fe_3O_4	0.045 mmol/g 0.596 mmol/g	0.040 mmol/g 0.563 mmol/g	[77]
$MnFe_2O4$@SiO_2@Vinyltrimethylsilane (VTMS) nanocomposite hydrogel	131	126	[78]
Fe_3O_4@SiO_2@Carboxyl-Terminated PAMAM Dendrimer Nanocomposite	117	115.82	[79]
NH_2-MCM-41	57.74 (ternary Ni(II) + Pb(II) + Cd(II) solns)	18.25 (ternary Ni(II) + Pb(II) + Cd(II) solns)	[80]
Magnetic melamine-MCM-48	127.24	114.08	[81]
SH-mSi@Fe_3O_4	91.5		[82]
Hierarchically macro/mesoporous hybrid silica spheres	81.9	33.4	[83]
Amino-functionalized Fe_3O_4@mesoporous SiO_2 core-shell composite microspheres NH_2-MS	128.21	51.81	[84]
SiO_2@Saponin	159.6 (Pb(II) solution) 94.52 (Pb(II) + Cd(II) solns)	124.5 (Cd(II) solution) 75.22 (Pb(II) + Cd(II) solns)	This study
meso-SiO_2	152.9 (Pb(II) solution) 85.47 (Pb(II) + Cd(II) solns)	114.1 (Cd(II) solution) 62.93 (Pb(II) + Cd(II) solns)	This study

4. Conclusions

Porous silica was prepared using the sol–gel method using a biosurfactant structure-directing agent saponin and TEOS (tetraethoxysilane) as a silica (SiO_2) precursor. The surface and morphology of the two as-prepared adsorbent materials, SiO_2@Saponin, and meso-SiO_2, were analyzed by SEM and TEM/HRTEM images, and it was found that the materials are composed of non-uniform aggregates of relatively large particles, with rigid, lamellar structures and meso-SiO_2 has a wormlike mesoporous structure, with uniform, homogeneously distributed mesopores. The textural parameters were determined from the nitrogen adsorption–desorption isotherms. Surprisingly, meso-SiO_2 has a smaller specific surface area than that of the SiO_2@saponin adsorbent, which is probably due to the fusion of micropores and smallest mesopores upon the calcination at 550 °C carried out for the removal of the saponin templating agent and obtaining of meso-SiO_2.

Batch experiments performed on the removal of Pb(II)/Cd(II) ions from single and binary aqueous solutions also led to the conclusion that SiO_2@Saponin has a higher adsorption capacity than meso-SiO_2 and we attributed this fact to both the favorable interactions

between carboxyl and hydroxyl functional groups of saponin and metal ions and its large specific surface area.

All the parameters (pH, contact time, retention capacity) and the Langmuir and Freundlich adsorption isotherms and kinetic models describing the adsorption processes of Pb(II)/Cd(II) ions onto these new silica adsorbents have been assessed for sorption of these metal ions from single and binary solutions. Our findings contribute to new knowledge related to the phenomena that occur in the adsorption of heavy metal ions from multicomponent solutions, a process extremely useful for the remediation of wastewater. The results of the competitive adsorption indicated the strong inhibitive effect of Pb(II) on the Cd(II) removal from binary solutions by adsorption onto meso-SiO_2, and in the case of SiO_2@Saponin, the stronger effect has been manifested by the Cd(II) ions. The values of the maximum adsorption capacities for Pb(II)/Cd(II), from single and binary solutions, onto SiO_2@Saponin and meso-SiO_2 recommend the application of both silica adsorbents in the removal of these metal ions from wastewater.

Supplementary Materials: The following supporting information can be downloaded at https://www.mdpi.com/article/10.3390/jcs8060227/s1, Figure S1: Linear Langmuir isotherm for Pd(II) adsorption on SiO_2@Saponin (a), meso-SiO_2 (b) and Cd(II) adsorption on SiO_2@Saponin (c), meso-SiO_2 (d)from single solutions.

Author Contributions: Conceptualization, F.D. and C.-M.S.; methodology, F.D. and C.-M.S.; formal analysis, F.D., C.-M.S., A.R., D.C.C., O.O., R.T., and E.V.; investigation, F.D., C.-M.S., and B.Z.; writing—original draft preparation, F.D., C.-M.S., D.C.C., and O.O.; writing—review and editing, F.D., C.-M.S., D.C.C., and O.O. All authors have read and agreed to the published version of the manuscript.

Funding: This research received no external funding.

Data Availability Statement: Research data are available upon request.

Acknowledgments: The authors are grateful to the Romanian Government for providing access to the research infrastructure of the National Center for Micro and Nanomaterials through the National Program titled "Installations and Strategic Objectives of National Interest".

Conflicts of Interest: The authors declare no conflicts of interest.

References

1. Huy, D.H.; Seelen, E.; Liem-Nguyen, V. Removal mechanisms of cadmium and lead ions in contaminated water by stainless steel slag obtained from scrap metal recycling. *J. Water Process. Eng.* **2020**, *36*, 101369. [CrossRef]
2. WHO. *Guidelines for Drinking-Water Quality—Fourth Edition Incorporating the First and Second Addenda*; WHO: Geneva, Switzerland, 2022.
3. Jaishankar, M.; Tseten, T.; Anbalagan, N.; Mathew, B.B.; Beeregowda, K.N. Toxicity, mechanism and health effects of some heavy metals. *Interdiscip. Toxicol.* **2014**, *7*, 60–72. [CrossRef] [PubMed]
4. Benoff, S.; Jacob, A.; Hurley, I.R. Male infertility and environmental exposure to lead and cadmium. *Hum. Reprod. Update* **2000**, *6*, 107–121. [CrossRef] [PubMed]
5. Simonescu, C.M.; Mason, T.J.; Călinescu, I.; Lavric, V.; Vînătoru, M.; Melinescu, A.; Culiţă, D.C. Ultrasound assisted preparation of calcium alginate beads to improve absorption of Pb^{+2} from water. *Ultrason. Sonochem.* **2020**, *68*, 105191. [CrossRef] [PubMed]
6. Zhang, Z.; Wang, T.; Zhang, H.; Liu, Y.; Xing, B. Adsorption of Pb(II) and Cd(II) by magnetic activated carbon and its mechanism. *Sci. Total Environ.* **2021**, *757*, 143910. [CrossRef] [PubMed]
7. Huang, R.; Lin, Q.; Zhong, Q.; Zhang, X.; Wen, X.; Luo, H. Removal of Cd(II) and Pb(II) from aqueous solution by modified attapulgite clay. *Arab. J. Chem.* **2020**, *13*, 4994–5008. [CrossRef]
8. Joseph, I.V.; Tosheva, L.; Doyle, A.M. Simultaneous removal of Cd(II), Co(II), Cu(II), Pb(II), and Zn(II) ions from aqueous solutions via adsorption on FAU-type zeolites prepared from coal fly ash. *J. Environ. Chem. Eng.* **2020**, *8*, 103895. [CrossRef]
9. Zhang, S.; Lv, T.; Mu, Y.; Zheng, J.; Meng, C. High adsorption of Cd(II) by modification of synthetic zeolites Y, A and mordenite with thiourea. *Chin. J. Chem. Eng.* **2020**, *28*, 3117–3125. [CrossRef]
10. Simonescu, C.M.; Culita, D.C.; Marinescu, V.; Tardei, C.; Talpeanu, D. Hydroxyapatite nanoparticles for acidic mine waters remediation. *Rev. Chim.* **2019**, *70*, 3167–3175. [CrossRef]
11. Amrulloh, H.; Kurniawan, Y.S.; Ichsan, C.; Jelita, J.; Simanjuntak, W.; Situmeang, R.T.M.; Krisbiantoro, P.A. Highly efficient removal of Pb(II) and Cd(II) ions using magnesium hydroxide nanostructure prepared from seawater bittern by electrochemical method. *Colloids Surf. A Physicochem. Eng. Asp.* **2021**, *631*, 127687. [CrossRef]

12. Solic, M.; Maletic, S.; Isakovski, M.K.; Nikic, J.; Watson, M.; Konya, Z.; Roncevic, S.D.S. Removing low levels of Cd(II) and Pb(II) by adsorption on two types of oxidized multiwalled carbon nanotubes. *J. Environ. Chem. Eng.* **2021**, *9*, 105402. [CrossRef]
13. Xiong, C.; Wang, W.; Tan, F.; Luo, F.; Chen, J.; Qiao, X. Investigation on the efficiency and mechanism of Cd(II) and Pb(II) removal from aqueous solutions using MgO nanoparticles. *J. Hazard. Mater.* **2015**, *299*, 664–674. [CrossRef] [PubMed]
14. Xue, Y.; Teng, W.; Chen, Y.; Ma, Q.; Chen, X.; Sun, Y.; Fan, J.; Qiu, Y.; Fu, R. Amorphous Mn-La oxides immobilized on carbon sphere for efficient removal of As(V), Cd(II), and Pb(II): Co-adsorption and roles of Mn species. *Chem. Eng. J.* **2022**, *429*, 132262. [CrossRef]
15. Valenzuela, F.; Quintana, G.; Briso, A.; Ide, V.; Basualto, C.; Gaete, J.; Montes, G. Cu(II), Cd(II), Pb(II) and As(V) adsorption from aqueous solutions using magnetic iron-modified calcium silicate hydrate: Adsorption kinetic analysis. *J. Water Process. Eng.* **2021**, *40*, 101951. [CrossRef]
16. Enache, D.; Vasile, E.; Simonescu, C.M.; Culiță, D.C.; Vasile, E.; Oprea, O.C.; Pandele, A.M.; Răzvan, A.; Dumitru, F.; Nechifor, G. Schiff base-functionalized mesoporous silicas (MCM-41, HMS) as Pb(II) adsorbents. *RSC Adv.* **2018**, *8*, 176–189. [CrossRef]
17. Culita, D.C.; Simonescu, C.M.; Patescu, R.E.; Stanica, N. Chitosan-based magnetic composites-efficient adsorbents for removal of Pb(II) and Cu(II) from aqueous mono and bicomponent solutions. *Rev. Chim.* **2018**, *69*, 2323–2330. [CrossRef]
18. Culita, D.C.; Simonescu, C.M.; Patescu, R.-E.; Dragne, M.; Stanica, N.; Oprea, O. o-Vanillin functionalized mesoporous silica—Coated magnetite nanoparticles for efficient removal of Pb(II) from water. *J. Solid State Chem.* **2016**, *238*, 311–320. [CrossRef]
19. Enache, D.F.; Vasile, E.; Simonescu, C.M.; Răzvan, A.; Nicolescu, A.; Nechifor, A.-C.; Oprea, O.; Pătescu, R.-E.; Onose, C.; Dumitru, F. Cysteine-functionalized silica-coated magnetite nanoparticles as potential nanoadsorbents. *J. Solid State Chem.* **2017**, *253*, 318–328. [CrossRef]
20. Santos, T.J.; Paggiaro, J.; Cabral Silva Pimentel, H.D.; Karla dos Santos Pereira, A.; Cavallini, G.S.; Pereira, D.H. Computational study of the interaction of heavy metal ions, Cd(II), Hg(II), and Pb(II) on lignin matrices. *J. Mol. Graph. Model.* **2022**, *111*, 108080. [CrossRef]
21. Chen, M.; Yu, M.; Kang, R.; Sun, H.; Zhang, W.; Wang, S.; Wang, N.; Wang, J. Removal of Pb(II) and V(V) from aqueous solution by glutaraldehyde crosslinked chitosan and nanocomposites. *Chemosphere* **2022**, *297*, 134084. [CrossRef]
22. Lan, T.; Guo, S.; Li, X.; Guo, J.; Bai, T.; Zhao, Q.; Yang, W.; Li, P. Mixed precursor geopolymer synthesis for removal of Pb(II) and Cd(II). *Mater. Lett.* **2020**, *274*, 127977. [CrossRef]
23. Huang, Z.; Xiong, C.; Ying, L.; Wang, W.; Wang, S.; Ding, J.; Lu, J. A post-functional Ti-based MOFs composite for selective removal of Pb(II) from water. *J. Hazard. Mater.* **2022**, *432*, 128700. [CrossRef]
24. Wang, Q.; Wang, Y.; Yang, Z.; Han, W.; Yuan, L.; Zhang, L.; Huang, X. Efficient removal of Pb(II) and Cd(II) from aqueous solutions by mango seed biosorbent. *Chem. Eng. J. Adv.* **2022**, *11*, 100295. [CrossRef]
25. Chen, M.; Wang, X.; Zhang, H. Comparative research on selective adsorption of Pb(II) by biosorbents prepared by two kinds of modifying waste biomass: Highly-efficient performance, application and mechanism. *J. Environ. Manag.* **2021**, *288*, 112388. [CrossRef] [PubMed]
26. Soria-Aguilar, M.D.J.; Martínez-Luévanos, A.; Sánchez-Castillo, M.A.; Carrillo-Pedroza, F.R.; Toro, N.; Narváez-García, V.M. Removal of Pb(II) from aqueous solutions by using steelmaking industry wastes: Effect of blast furnace dust's chemical composition. *Arab. J. Chem.* **2021**, *14*, 103061. [CrossRef]
27. Dudarko, O.; Kobylinska, N.; Mishra, B.; Kessler, V.G.; Tripathi, B.P.; Seisenbaeva, G.A. Facile strategies for synthesis of functionalized mesoporous silicas for the removal of rare-earth elements and heavy metals from aqueous systems. *Microporous Mesoporous Mater.* **2021**, *315*, 110919. [CrossRef]
28. Noreen, S.; Maqbool, A.; Maqbool, I.; Shafique, A.; Khan, M.M.; Junejo, Y.; Ahmed, B.; Anwar, M.; Majeed, A.; Abbas, M.; et al. Multifunctional mesoporous silica-based nanocomposites: Synthesis and biomedical applications. *Mater. Chem. Phys.* **2022**, *285*, 126132. [CrossRef]
29. Xie, Y.; Kocaefe, D.; Chen, C.; Kocaefe, Y. Review of Research on Template Methods for Nanomaterials. *J. Nanomater.* **2016**, *2016*, 2302595. [CrossRef]
30. Grozdov, D.; Zinicovscaia, I. Mesoporous Materials for Metal-Laden Wastewater Treatment. *Materials* **2023**, *16*, 5864. [CrossRef]
31. Khalifa, M.E.; Abdelrahman, E.A.; Hassanien, M.M.; Ibrahim, W.A. Application of Mesoporous Silica Nanoparticles Modified with Dibenzoylmethane as a Novel Composite for Efficient Removal of Cd(II), Hg(II), and Cu(II) Ions from Aqueous Media. *J. Inorg. Organomet. Polym. Mater.* **2020**, *30*, 2182–2196. [CrossRef]
32. Li, S.; Li, S.; Wen, N.; Wei, D.; Dong, W.; Zhang, Y. Highly effective removal of lead and cadmium ions from wastewater by bifunctional magnetic mesoporous silica. *Sep. Purif. Technol.* **2021**, *265*, 118341. [CrossRef]
33. Kregiel, D.; Berlowska, J.; Witonska, I.; Antolak, H.; Proestos, C.; Babic, M.; Babic, L.; Zhang, B. Saponin-Based, Biological-Active Surfactants from Plants. In *Application and Characterization of Surfactants*; Najjar, R., Ed.; InTech: London, UK, 2017. [CrossRef]
34. McClements, D.J.; Gumus, C.E. Natural emulsifiers—Biosurfactants, phospholipids, biopolymers, and colloidal particles: Molecular and physicochemical basis of functional performance. *Adv. Colloid Interface Sci.* **2016**, *234*, 3–26. [CrossRef] [PubMed]
35. Zhou, W.; Yang, J.; Lou, L.; Zhu, L. Solubilization properties of polycyclic aromatic hydrocarbons by saponin, a plant-derived biosurfactant. *Environ. Pollut.* **2011**, *159*, 1198–1204. [CrossRef] [PubMed]
36. Liu, Z.; Li, Z.; Zhong, H.; Zeng, G.; Liang, Y.; Chen, M.; Wu, Z.; Zhou, Y.; Yu, M.; Shao, B. Recent advances in the environmental applications of biosurfactant saponins: A review. *J. Environ. Chem. Eng.* **2017**, *5*, 6030–6038. [CrossRef]

37. Samal, K.; Das, C.; Mohanty, K. Application of saponin biosurfactant and its recovery in the MEUF process for removal of methyl violet from wastewater. *J. Environ. Manag.* **2017**, *203*, 8–16. [CrossRef] [PubMed]
38. Song, S.; Zhu, L.; Zhou, W. Simultaneous removal of phenanthrene and cadmium from contaminated soils by saponin, a plant-derived biosurfactant. *Environ. Pollut.* **2008**, *156*, 1368–1370. [CrossRef] [PubMed]
39. Pei, G.; Zhu, Y.; Cai, X.; Shi, W.; Li, H. Surfactant flushing remediation of o-dichlorobenzene and p-dichlorobenzene contaminated soil. *Chemosphere* **2017**, *185*, 1112–1121. [CrossRef] [PubMed]
40. Li, Q.; Zhong, H.; Cao, Y. Effective extraction and recovery of rare earth elements (REEs) in contaminated soils using a reusable biosurfactant. *Chemosphere* **2020**, *256*, 127070. [CrossRef]
41. Samal, K.; Das, C.; Mohanty, K. Eco-friendly biosurfactant saponin for the solubilization of cationic and anionic dyes in aqueous system. *Dye Pigment* **2017**, *140*, 100–108. [CrossRef]
42. Tang, J.; He, J.; Liu, T.; Xin, X. Removal of heavy metals with sequential sludge washing techniques using saponin: Optimization conditions, kinetics, removal effectiveness, binding intensity, mobility and mechanism. *RSC Adv.* **2017**, *7*, 33385–33401. [CrossRef]
43. Rai, S.; Acharya-Siwakoti, E.; Kafle, A.; Devkota, H.P.; Bhattarai, A. Plant-Derived Saponins: A Review of Their Surfactant Properties and Applications. *Science* **2021**, *3*, 44. [CrossRef]
44. Croizet-Berger, B.K.K.; Delemeule, M.; Estager, J.; Mannu, N. Silices Mesoporeuses et leur Procede de Synthese. WO/2017/182245, 26 October 2017.
45. Korchowiec, B.; Gorczyca, M.; Wojszko, K.; Janikowska, M.; Henry, M.; Rogalska, E. Impact of two different saponins on the organization of model lipid membranes. *Biochim. Biophys. Acta-Biomembr.* **2015**, *1848*, 1963–1973. [CrossRef] [PubMed]
46. Lorent, J.H.; Quetin-Leclercq, J.; Mingeot-Leclercq, M.P. The amphiphilic nature of saponins and their effects on artificial and biological membranes and potential consequences for red blood and cancer cells. *Org. Biomol. Chem.* **2014**, *12*, 8803–8822. [CrossRef] [PubMed]
47. Oleszek, W.; Hamed, A. Saponin-Based Surfactants. In *Surfactants from Renewable Resources*; Kjellin, M., Johansson, I., Eds.; John Wiley & Sons, Ltd.: Hoboken, NJ, USA, 2010; Chapter 12; pp. 239–249. [CrossRef]
48. Böttcher, S. Interfacial Properties of Saponins from Quillajasaponaria Molina and Their Functionality in Dispersed Systems. Ph.D. Thesis, Technische Universität, Berlin, Germany, 2017. Available online: https://depositonce.tu-berlin.de//handle/11303/6734%0Ahttp://files/134/B%C3%B6ttcher (accessed on 1 February 2024).
49. Mitra, S.; Dungan, S.R. Micellar Properties of Quillaja Saponin. 1. Effects of Temperature, Salt, and pH on Solution Properties. *J. Agric. Food Chem.* **1997**, *45*, 1587–1595. [CrossRef]
50. Raffa, P. Design and Synthesis of Low Molecular Weight and Polymeric Surfactants for Enhanced Oil Recovery. In *Surfactants in Upstream E&P. Petroleum Engineering*; Solling, T., Shahzad Kamal, M., Shakil Hussain, S.M., Eds.; Springer: Cham, Switzerland, 2021; pp. 3–40. [CrossRef]
51. Schmitt, C.; Grassl, B.; Lespes, G.; Desbrières, J.; Pellerin, V.; Reynaud, S.; Gigault, J.; Hackley, V.A. Saponins: A renewable and biodegradable surfactant from its microwave-assisted extraction to the synthesis of monodisperse lattices. *Biomacromolecules* **2014**, *15*, 856–862. [CrossRef] [PubMed]
52. Amarowicz, R.; Pegg, R.B.; Okubo, K. Fourier Transform InfraRed (FTIR) spectra of soybean saponin Ab and Bb. *Mol. Nutr. Food Res.* **1996**, *40*, 342–343. [CrossRef]
53. Gunde, M.K. Vibrational modes in amorphous silicon dioxide. *Phys. B Condens. Matter.* **2000**, *292*, 286–295. [CrossRef]
54. Thommes, M.; Kaneko, K.; Neimark, A.V.; Olivier, J.P.; Rodriguez-Reinoso, F.; Rouquerol, J.; Sing, K.S.W. Physisorption of Gases with Special Reference to the Evaluation of Surface Area and Pore Size Distribution (IUPAC Technical Report). *Pure Appl. Chem.* **2015**, *87*, 1051–1069. [CrossRef]
55. Schlumberger, C.; Thommes, M. Characterization of Hierarchically Ordered Porous Materials by Physisorption and Mercury Porosimetry—A Tutorial Review. *Adv. Mater. Inter.* **2021**, *8*, 2002181. [CrossRef]
56. Sumanjeet, K.; Neeta, S.; Manpreet, K. Single and Competitive Removal of Pb(II) in the Presence of Ni(II) using Polyacrylamide Grafted Rice Husk. *J. Appl. Sci. Environ. Manag.* **2023**, *27*, 63–70. [CrossRef]
57. Verma, A.; Agarwal, M.; Sharma, S.; Singh, N. Competitive removal of cadmium and lead ions from synthetic wastewater using *Kappaphycus striatum*. *Environ. Nanotechnol. Monit. Manag.* **2021**, *15*, 100449. [CrossRef]
58. Ifijen, I.H.; Itua, A.B.; Maliki, M.; Ize-Iyamu, C.O.; Omorogbe, S.O.; Aigbodion, A.I.; Ikhuoria, E.U. The removal of nickel and lead ions from aqueous solutions using green synthesized silica microparticles. *Heliyon* **2020**, *6*, e04907. [CrossRef] [PubMed]
59. Sajid, M.; Kabeer, M.; Younas, M.; Ihsanullah, I.; Baig, N. *Conocarpuslancifolius* Leaves as Low-Cost, Green and Sustainable Sorbent Material for Simultaneous Removal of Cadmium, Chromium, and Lead Ions from Aqueous Samples. *Arab. J. Sci. Eng.* **2024**, *49*, 613–621. [CrossRef]
60. Lian, W.; Yang, L.; Joseph, S.; Shi, W.; Bian, R.; Zheng, J.; Li, L.; Shan, S.; Pan, G. Utilization of biochar produced from invasive plant species to efficiently adsorb Cd (II) and Pb (II). *Bioresour. Technol.* **2020**, *317*, 124011. [CrossRef] [PubMed]
61. Yadav, A.; Bagotia, N.; Sharma, A.K.; Kumar, S. Simultaneous adsorptive removal of conventional and emerging contaminants in multi-component systems for wastewater remediation: A critical review. *Sci. Total Environ.* **2021**, *799*, 149500. [CrossRef] [PubMed]
62. Sangeetha, K.; Vidhya, G.; Vasugi, G.; Girija, G.V.E.K. Lead and cadmium removal from single and binary metal ion solution by novel hydroxyapatite/alginate/gelatin nanocomposites. *J. Environ. Chem. Eng.* **2018**, *6*, 1118–1126. [CrossRef]
63. Foo, K.Y.; Hameed, B.H. Insights into the modeling of adsorption isotherm systems. *Chem. Eng. J.* **2010**, *156*, 2–10. [CrossRef]

64. Langmuir, I. The constitution and fundamental properties of solids and liquids. Part II.—Liquids. *J. Frankl. Inst.* **1917**, *184*, 721. [CrossRef]
65. Weber, W.J., Jr.; Digiano, F.A. *Process dynamics in Environmental Systems*, 1st ed.; John Wily and Sons: Hoboken, NJ, USA, 1996.
66. Ramsenthil, R.; Meyyappan, R.M. Single and multi-component biosorption of copper and zinc ions using micro algal resin. *Int. J. Environ. Sci. Dev.* **2010**, *1*, 298–301. [CrossRef]
67. Nharingo, T.; Ngwenya, J.T. Single and Binary sorption of lead(II) and zinc(II) ions onto *Eichhornia Crassipes* (water hyacinth) ash. *Int. J. Eng. Sci. Innov. Technol. (IJESIT)* **2013**, *2*, 419–426.
68. Mahamadi, C.; Nharingo, T. Competitive adsorption of Pb^{2+}, Cd^{2+} and Zn^{2+} ions onto *Eichhornia crassipes* in binary and ternary systems. *Bioresour. Technol.* **2010**, *101*, 859–864. [CrossRef]
69. Chen, D.; Zeng, Z.; Zeng, Y.; Zhang, F.; Wang, M. Removal of methylene blue and mechanism on magnetic γ-Fe_2O_3/SiO_2 nanocomposite from aqueous solution. *Water Resour. Ind.* **2016**, *15*, 1–13. [CrossRef]
70. Kypritidou, Z.; El-Bassi, L.; Jellali, S.; Kinigopoulou, V.; Tziritis, E.; Akrout, H.; Jeguirim, M.; Doulgeris, C. Lead removal from aqueous solutions by olive mill wastes derived biochar: Batch experiments and geochemical modelling. *J. Environ. Manag.* **2022**, *318*, 115562. [CrossRef] [PubMed]
71. El-Feky, H.H.; Behiry, M.S.; Amin, A.S.; Nassar, M.Y. Facile Fabrication of Nano-sized SiO_2 by an Improved Sol–Gel Route: As an Adsorbent for Enhanced Removal of Cd(II) and Pb(II) Ions. *J. Inorg. Organomet. Polym. Mater.* **2022**, *32*, 1129–1141. [CrossRef]
72. Ciesielczyk, F.; Bartczak, P.; Jesionowski, T. Removal of cadmium(II) and lead(II) ions from model aqueous solutions using sol–gel-derived inorganic oxide adsorbent. *Adsorption* **2016**, *22*, 445–458. [CrossRef]
73. Liu, Y.; Fu, R.; Sun, Y.; Zhou, X.; Baig, S.A.; Xu, X. Multifunctional nanocomposites Fe_3O_4@SiO_2-EDTA for Pb(II) and Cu(II) removal from aqueous solutions. *Appl. Surf. Sci.* **2016**, *369*, 267–276. [CrossRef]
74. Liu, Y.; Lou, Z.; Sun, Y.; Zhou, X.; Baig, S.A.; Xu, X. Influence of complexing agent on the removal of Pb(II) from aqueous solutions by modified mesoporous SiO_2. *Microporous Mesoporous Mater.* **2017**, *246*, 1–13. [CrossRef]
75. Wang, J.; Zheng, S.; Shao, Y.; Liu, J.; Xu, Z.; Zhu, D. Amino-functionalized Fe_3O_4@SiO_2 core-shell magnetic nanomaterial as a novel adsorbent for aqueous heavy metals removal. *J. Colloid Interface Sci.* **2010**, *349*, 293–299. [CrossRef]
76. Harinath, Y.; Reddy, D.H.K.; Sharma, L.S.; Seshaiah, K. Development of hyperbranched polymer encapsulated magnetic adsorbent (Fe_3O_4@SiO_2-NH_2-PAA) and its application for decontamination of heavy metal ions. *J. Environ. Chem. Eng.* **2017**, *5*, 4994–5001. [CrossRef]
77. Ren, Y.; Abbood, H.A.; He, F.; Peng, H.; Huang, K. Magnetic EDTA-modified chitosan/SiO_2/Fe_3O_4 adsorbent: Preparation, characterization, and application in heavy metal adsorption. *Chem. Eng. J.* **2013**, *226*, 300–311. [CrossRef]
78. Ghobadifar, V.; Marandi, G.B.; Kurdtabar, M.; Bardajee, G.R. Removal of Pb(II) and Cd(II) by $MnFe_2O_4$@SiO_2@VTMS Nanocomposite Hydrogel from Aqueous Solutions. *J. Polym. Environ.* **2023**, *31*, 2686–2704. [CrossRef]
79. Zarei, A.; Saedi, S.; Seidi, F. Synthesis and Application of Fe_3O_4@SiO_2@Carboxyl-Terminated PAMAM Dendrimer Nanocomposite for Heavy Metal Removal. *J. Inorg. Organomet. Polym. Mater.* **2018**, *28*, 2835–2843. [CrossRef]
80. Heidari, A.; Younesi, H.; Mehraban, Z. Removal of Ni(II), Cd(II), and Pb(II) from a ternary aqueous solution by amino functionalized mesoporous and nano mesoporous silica. *Chem. Eng. J.* **2009**, *153*, 70–79. [CrossRef]
81. Anbia, M.; Kargosha, K.; Khoshbooei, S. Heavy metal ions removal from aqueous media by modified magnetic mesoporous silica MCM-48. *Chem. Eng. Res. Des.* **2015**, *93*, 779–788. [CrossRef]
82. Li, G.; Zhao, Z.; Liu, J.; Jiang, G. Effective heavy metal removal from aqueous systems by thiol functionalized magnetic mesoporous silica. *J. Hazard. Mater.* **2011**, *192*, 277–283. [CrossRef] [PubMed]
83. Li, Z.Y.; Wang, X.P.; Luo, Z.Y.; Xue, Y.W.; Shi, Z.G. Hierarchically macro/mesoporous hybrid silica spheres for fast capture of heavy metal ions. *Mater. Lett.* **2014**, *128*, 140–143. [CrossRef]
84. Tang, Y.; Liang, S.; Wang, J.; Yu, S.; Wang, Y. Amino-functionalized core-shell magnetic mesoporous composite microspheres for Pb(II) and Cd(II) removal. *J. Environ. Sci.* **2013**, *25*, 830–837. [CrossRef]